Postprint of: Koziel S., Pietrenko-Dabrowska A., Rapid multi-objective optimization of antennas using nested kriging surrogates and single-fidelity EM simulation models", Engineering Computations, Vol. 37 No. 4 (2019), pp. 1491-1512. DOI: 10.1108/EC-05-2019-0200

Rapid Multi-Objective Optimization of Antennas Using Nested Kriging Surrogates and Single-Fidelity EM Simulation Models

Slawomir Koziel[1,2] and Anna Pietrenko-Dabrowska[2]

[1] Engineering Optimization & Modeling Center, Reykjavik University, 101 Reykjavik, Iceland, koziel@ru.is

[2] Faculty of Electronics, Telecommunications and Informatics, Gdansk University of Technology, 80-233 Gdansk, Poland, anna.dabrowska@pg.edu.pl

Rapid Multi-Objective Optimization of Antennas Using Nested Kriging Surrogates and Single-Fidelity EM Simulation Models

Keywords: Antenna design, multi-objective design, surrogate modeling, simulation-driven design, kriging interpolation, design trade-offs.

Structured Abstract

Purpose

A computationally efficient framework for multi-objective optimization (MO) of antennas involving nested kriging modeling technology is proposed. The technique is demonstrated through a two-objective optimization of a planar Yagi antenna and three-objective design of a compact wideband antenna.

Design/methodology/approach

The keystone of the proposed approach is the employment of recently introduced nested kriging modeling for identifying the design space region containing the Pareto front and constructing fast surrogate model for the MO algorithm. Surrogate-assisted design refinement is applied to improve the accuracy of Pareto set determination. Consequently, the Pareto set is obtained cost-efficiently, even though the optimization process utilizes solely high-fidelity electromagnetic (EM) analysis.

Findings

The optimization cost is dramatically reduced for the proposed framework as compared to other state-of-the-art frameworks. The initial Pareto set is identified more

precisely (its span is wider and of better quality), which is a result of a considerably smaller domain of the nested kriging model and better predictive power of the surrogate.

Research limitations/implications

The proposed technique can be generalized to accommodate low- and high-fidelity EM simulations in a straightforward manner. The future work will incorporate variable-fidelity simulations in order to further reduce the cost of the training data acquisition.

Originality/value

The fast MO optimization procedure with the use of the nested kriging modeling technology for approximation of the Pareto set has been proposed and its superiority over state-of-the-art surrogate-assisted procedures has been proved. To our knowledge, this approach to multi-objective antenna optimization is novel and enables obtaining optimal designs cost-effectively even in relatively highly dimensional spaces (considering typical antenna design setups) within wide parameter ranges.

Abstract

Ever increasing performance requirements make the design of contemporary antenna systems a complex and multi-stage process. One of the challenges, pertinent to the emerging application areas but also some of the recent trends (miniaturization, demands for multi-functionality, etc.), is the necessity of handling several performance figures such as impedance matching, gain, or axial ratio, often over multiple frequency bands. The fundamental difficulty is that most of the design objectives are at least partially conflicting. Hence, an improvement of one generally implies degradation of the others. The knowledge of available trade-offs is indispensable and can be acquired through multi-objective optimization (MO). Unfortunately, MO is computationally expensive when executed at the level of EM simulation models, otherwise necessary from the standpoint of antenna evaluation reliability. This paper proposes a computationally efficient framework for MO of antennas. Its keystone is the recently introduced nested kriging modeling technology, here adopted for identifying the design space region that contains the best design trade-offs, as well as for constructing a fast surrogate model to be processed by the MO algorithm. The technique is demonstrated through a two-objective optimization of a planar Yagi antenna (with respect to the impedance matching and gain enhancement) and three-objective design of a compact wideband antenna (with respect to the impedance matching, gain variability, and the footprint area). In both cases, the Pareto set is obtained at the low cost of a few hundred of antenna simulations, even though the optimization process is exclusively based on high-fidelity EM analysis.

1. Introduction

Performance requirements imposed on contemporary antenna systems are multifold and pertinent to both electrical and field characteristics (Stutzman and Thiele, 2012), multi-band and multi-functional operation (Borhani *et al.*, 2016; Soltani *et al.*, 2017), as well as geometrical constraints (primarily compact size, Bhattacharya *et al.*, 2016). The need for fulfilling stringent specifications necessitates a development of antennas that feature more and more complex geometries and are described by a large number of variables (Matekovits *et al.*, 2007; Szini *et al.*, 2015; Buckley *et al.*, 2016). Both factors create the need for handling/optimizing several design objectives at the same time while operating within parameter spaces of ever-increasing number of dimensions. Utilization of full-wave electromagnetic (EM) simulation tools, computationally expensive but mandatory to ensure sufficient evaluation reliability, is yet another design challenge. Many of the design objectives are at least partially conflicting, i.e., improvement of one implies certain degradation of others. Perhaps the most recognized example is antenna miniaturization: reduction of the size normally leads to problems with ensuring sufficient impedance matching as well as affects other characteristics, such as efficiency or pattern stability (Liu *et al.*, 2014; Koziel *et al.*, 2018). Consequently, any practical design must be a compromise (or trade-off) between the objectives of interest.

The most reliable way of handling multiple goals (as well as just one objective for that matter) is numerical optimization (Deb and Gupta, 2006). Majority of practically utilized algorithms are single-objective routines (Tian *et al.*, 2010; Koziel and Ogurtsov, 2014). These, however, require a scalar cost function. In order to control several design goals, some sort of aggregation (e.g., using a weighted sum approach), or constrained

optimization with acceptance levels set for all but the primary objective, need to be performed. In either case, the outcome is a single design that qualitatively (but not necessarily quantitatively) represents the designer's preferences about the goals. On the other hand, genuine multi-objective optimization (MO) procedures are capable of identifying the entire set of trade-off designs (the Pareto set, Koziel and Bekasiewicz, 2016). The most popular class of MO algorithms involve population-based metaheuristics (Darvish and Ebrahimzadeh, 2018; Goudos *et al.*, 2011; Bauernfeind *et al.*, 2017; Jayaprakasam *et al.*, 2014; Aravanis *et al.*, 2015; Rinaldo *et al.*, 2005), which exhibit global search capabilities (important in some cases), but come at the expense of a tremendous computational cost (Easum *et al.*, 2018; Nagar and Werner, 2018). The latter is normally unmanageable if the antenna performance is evaluated through EM simulation. A new approach to expedited global design optimization of antennas with evolutionary algorithm by means of small-scale parallelizing computations has been reported recently (Akinsolu *et al.*, 2019; Liu *et al.*, 2018), yet the method has been applied to single-objective optimization problems only.

It seems that utilization of surrogate models is currently the most promising approach to render EM-driven MO procedures computationally feasible (Koziel and Bekasiewicz, 2016). In relatively simple cases (in terms of the parameter space dimensionality), construction of global surrogates may be sufficient (Chen, 2015; de Villiers *et al.*, 2017; Easum *et al.*, 2017). For other situations (>10 geometry parameters) more needs to be done. Some of the recently proposed techniques (Koziel and Ogurtsov, 2013; Koziel *et al.*, 2014a), suggest utilization of variable-fidelity EM simulations along with the initial design space reduction. The latter aims at identifying the region of the

parameter space that contains the Pareto front and at constructing the surrogate therein. This has been demonstrated to yield considerable computational savings even though the applied space reduction methods only give a very rough estimation of the Pareto front geometry.

In this paper, a novel multi-optimization framework is proposed for a cost-efficient EM-driven antenna design. Our methodology adopts a recently reported nested kriging surrogate modeling technique (Koziel and Pietrenko-Dabrowska, 2019). The technique utilizes two kriging surrogates. The first-level model is employed to define the domain of the surrogate, containing the designs that are of high-quality from the point of view of the performance figures relevant to the considered system. The second-level model, set up in that domain, is the actual surrogate representing the system outputs. The fundamental benefit of constraining the surrogate domain is a notable reduction of the required training data set as compared to the traditional kriging approach over a box-constrained domain. Here, nested kriging methodology is used to identify the parameter space region containing the Pareto set (design space reduction) as well as to construct the surrogate that allows us to produce the initial approximation of the trade-off designs through metaheuristic optimization. Due to a good precision of representing the Pareto front geometry by the nested kriging framework, the MO process can be executed in a computationally efficient manner in spite of merely utilizing high-fidelity EM simulations of the antenna at hand. For the sake of demonstration, two structures are optimized, a planar Yagi antenna (for best matching and maximum gain), and a wideband monopole (for best matching, minimum gain variability, and minimum size). In both cases, the Pareto set is obtained at

the cost of only a few hundred of EM simulations, which is almost 80-percent less than for the surrogate-assisted framework involving a simpler design space reduction technique.

This paper is the first attempt to employ the nested kriging method for multi-objective optimization. The major novelty is in adopting the nested kriging technique for design space confinement and providing a fast surrogate for low-cost generation of the initial Pareto set. For that purpose, a rigorous mathematical formalism is developed in Section 2.4, which permits the establishment of the surrogate in an arbitrary subset of the objective space instead of the box-constrained space as in Koziel and Pietrenko-Dabrowska, 2019. The presented methodology is demonstrated to efficiently solve MO of real-world antenna design tasks. In addition, its superiority over state-of-the-art surrogate-assisted procedures is validated. The proposed method is generic in the sense of its capability of handling any number of design objectives.

2. Antenna Optimization with Multiple Objectives Aided by Nested Kriging Surrogates

This section provides a necessary background material concerning multi-objective optimization by means of surrogate modeling. It also briefly recalls the concept of nested kriging, as well as describes how to incorporate it into the multi-objective design framework. The main goal is a reduction of the computational overhead of multi-objective design beyond what is offered by the existing approaches.

2.1. Multi-Objective Optimization Using Surrogate Models

For the purpose of further considerations, the design objectives will be denoted as F_k, $k = 1, \ldots, N_{obj}$, where N_{obj} stands for the overall number of the goals. Multi-objective optimization (MO) aims at finding a Pareto set of designs that are globally non-dominated

(Deb, 2001). A design is globally non-dominated—within the considered parameter space— if there is no other design simultaneously better with respect to all objectives. The Pareto set represents the best possible trade-offs with respect to $[F_1\ F_2\ \ldots\ F_{Nobj}]$.

The antenna under design is evaluated using EM analysis and the respective computational model is denoted as $\boldsymbol{R}(\boldsymbol{x})$, where $\boldsymbol{x}$ is a vector of adjustable (typically, geometry) parameters. As explained in Section 1, it is impractical or even infeasible to carry out MO directly on $\boldsymbol{R}$ when using population-based metaheuristics. According to the recent literature (de Villiers *et al.*, 2017; Easum *et al.*, 2017; Koziel and Ogurtsov, 2013; Koziel *et al.*, 2014a), the most promising way of speeding up the optimization process is a utilization of an auxiliary surrogate model $\boldsymbol{R}_s$ (a faster representation of the antenna at hand). In most cases, the surrogate is an approximation model, typically a kriging (An *et al.*, 2018) or Gaussian process regression one (Lyu *et al.*, 2018). Other approximation methods may also be used, e.g., artificial neural networks (ANNs; Mishra *et al.*, 2015) or support vector regression (SVR; Jacobs, 2012). A particular selection of the modeling framework is generally of secondary importance, although particular techniques may suffer from certain issues. For example, the generalization ability of ANNs, i.e., the predictive power over the points outside the training set, may proof deficient (Chauchan *et al.*, 2012). Handling this issue generally requires appropriate adjustment of the network architecture (Na *et al.*, 2017). On the other hand, SVR's superior generalization capabilities are superior over ANNS. Yet, developing effective antenna models using SVM is not a straightforward process, and the researchers have to employ their domain expertise in it (Chauchan *et al.*, 2012). Regardless of the approximation technique utilized, the surrogate can be optimized directly using, e.g., a multi-objective evolutionary algorithm (MOEA; Fonseca, 1995).

Further acceleration can be achieved by exploiting variable-fidelity EM simulations. This sort of approach has been adopted in Koziel and Ogurtsov, 2013 and Koziel *et al.*, 2014a, where the surrogate was constructed at the level of coarse-discretization EM model. Unfortunately, a refinement process is required to accommodate the discrepancies between the low- and high-fidelity simulations. In Koziel and Ogurtsov, 2013, a simple response correction in the form of output space mapping (Koziel *et al.*, 2008) has been used. The high-fidelity Pareto designs have been obtained through the following refinement of the selected low-fidelity Pareto-optimal designs $\boldsymbol{x}_s^{(k)}$

$$\boldsymbol{x}_f^{(k)} = \arg \min_{\substack{\boldsymbol{x},\, F_2(\boldsymbol{x}) \le F_2(\boldsymbol{x}_s^{(k)}) \\ \vdots \\ F_{N_{obj}}(\boldsymbol{x}) \le F_{N_{obj}}(\boldsymbol{x}_s^{(k)})}} F_1\left(\boldsymbol{R}_s(\boldsymbol{x}) + [\boldsymbol{R}(\boldsymbol{x}_s^{(k)}) - \boldsymbol{R}_s(\boldsymbol{x}_s^{(k)})]\right) \tag{1}$$

The correction term $\boldsymbol{R}(\boldsymbol{x}_s^{(k)}) - \boldsymbol{R}_s(\boldsymbol{x}_s^{(k)})$ ensures perfect alignment between the surrogate $\boldsymbol{R}_s$ and the high-fidelity model at $\boldsymbol{x}_s^{(k)}$ (Koziel and Ogurtsov, 2013). In Koziel *et al.*, 2014b, an alternative refinement procedure based on co-kriging has been proposed.

2.2. Reduction of Parameter Ranges

The fundamental difficulty concerning the surrogate-assisted MO, as described in Section 2.1, is a construction of the surrogate model itself. Apart from low-dimensional cases (up to a few parameters), it is simply not possible to build the model in the entire design space. The reasons include the lack of prior knowledge about the Pareto front location (which implies wide parameter ranges), and the curse of dimensionality. Both issues lead to excessive costs of training data acquisition.

The design space can be reduced in a reasonable manner by considering the single-objective optima $\boldsymbol{x}^{*(k)} = \text{argmin}\{\boldsymbol{x} : F_k(\boldsymbol{R}(\boldsymbol{x}))\}$, i.e., the extreme Pareto-optimal designs that determine the span of the Pareto front. Thus, the lower and upper bounds for the antenna

parameters can be set as $\boldsymbol{l}^* = \min\{\boldsymbol{x}^{*(1)},\ldots, \boldsymbol{x}^{*(N_{obj})}\}$ and $\boldsymbol{u}^* = \max\{\boldsymbol{x}^{*(1)},\ldots, \boldsymbol{x}^{*(N_{obj})}\}$ (Koziel and Ogurtsov, 2013). Apart from some "pathological" cases, the interval $[\boldsymbol{l}^*,\boldsymbol{u}^*]$ contains the vast majority of the Pareto front. A better idea about the Pareto front geometry can be acquired using more involved methods such as the rotational space reduction (Koziel and Bekasiewicz, 2015), which is, however, applicable to two-objective problems only.

2.3. Surrogate Modeling Using Nested Kriging

This work aims at the development of an improved surrogate-assisted MO procedure, which permits further computational savings over the framework described in Sections 2.1 and 2.2. To this end, we adopt a recently reported nested kriging modelling (Koziel and Pietrenko-Dabrowska, 2019). It is used to implement a more efficient design space reduction scheme and to construct the surrogate model for initial Pareto set identification. The term "nested" refers to performing kriging interpolation consecutively twice: first to identify the surrogate model domain, then to establish the actual surrogate model itself in the constrained domain. The difference between the nested and traditional kriging is that the latter operates in an interval-like domain, defined by lower and upper parameter bounds. Due to complex interactions between geometry parameters, designs that are optimal with respect to the performance figures are focused within small subsets of such a domain (Koziel and Sigurdsson, 2017). Thus, constraining the surrogate model domain with the nested kriging, leads to significant cost savings. In this section, we briefly recall the nested modeling concept, whereas its adaptation for MO purposes is explained in Section 2.4.

The figures of interest selected for the design process (e.g., operating frequency, bandwidth, maximum/average in-band gain, etc.) are denoted by f_k, $k = 1, \ldots, N$. These are

identical to the MO design goals F_k of Section 2.1. The foundation of the nested kriging are the reference designs $\boldsymbol{x}^{(j)} = [x_1^{(j)} \ldots x_n^{(j)}]^T$, $j = 1, \ldots, p$, optimized with respect to the performance vectors $\boldsymbol{f}^{(j)} = [f_1^{(j)} \ldots f_N^{(j)}]$. The vectors $\boldsymbol{f}^{(j)}$ are allocated within the objective space F defined using the ranges $f_{k.\min} \le f_k^{(j)} \le f_{k.\max}$, $k = 1, \ldots, N$, to be covered by the surrogate model (Koziel and Pietrenko-Dabrowska, 2019). Clearly, the coverage of the objective space should be possibly uniform. Typically, the number of the reference designs is small, e.g., around 10 or so (cf. Koziel and Pietrenko-Dabrowska, 2019) because the dimensionality of F is low.

The modeling procedure involves two surrogates. The first-level model $\boldsymbol{s}_I(\boldsymbol{f})$ maps F into the design space X. The model $\boldsymbol{s}_I$ interpolates the training data set $\{\boldsymbol{f}^{(j)}, \boldsymbol{x}^{(j)}\}$ using kriging (Simpson *et al.*, 2001), see Fig. 1. The image of F through $\boldsymbol{s}_I$, $\boldsymbol{s}_I(F) \subset X$, provides the first approximation of the surrogate model domain. This is the best information available from the reference points about the designs optimal with respect to $\boldsymbol{f} \in F$. Yet, this information is limited, and $\boldsymbol{s}_I(F)$ needs to be orthogonally extended towards its normal vectors to ensure that all of optimum designs are enclosed in the model domain. The normal extension vectors are denoted as $\boldsymbol{v}_n^{(k)}(\boldsymbol{f})$, $k = 1, \ldots, n - N$, and they are the functions of the performance vector $\boldsymbol{f}$ (Koziel and Pietrenko-Dabrowska, 2019). Let us also define: $\boldsymbol{x}_{\max} = \max\{\boldsymbol{x}^{(k)}, k = 1, \ldots, p\}$, $\boldsymbol{x}_{\min} = \min\{\boldsymbol{x}^{(k)}, k = 1, \ldots, p\}$, $\boldsymbol{x}_d = \boldsymbol{x}_{\max} - \boldsymbol{x}_{\min}$, as well as the extension coefficients

$$\boldsymbol{\alpha}(\boldsymbol{f}) = [\alpha_1(\boldsymbol{f}) \ldots \alpha_{n-N}(\boldsymbol{f})]^T = \frac{D}{2}\left[|\, \boldsymbol{x}_d \boldsymbol{v}_n^{(1)}(\boldsymbol{f})\,| \ \ldots\ |\, \boldsymbol{x}_d \boldsymbol{v}_n^{(n-N)}(\boldsymbol{f})\,|\right]^T \tag{2}$$

where D is a user-defined thickness parameter determining the orthogonal extension. It has been shown in Koziel and Pietrenko-Dabrowska, 2019, that the value of D affects the

model accuracy to certain extent, however, the predictive power dependence on D is not significant.

The model domain X_S is defined by the coefficients α_k, and it is located between the surfaces (or manifolds) M_+ and M_- (see Fig. 1(b))

$$M_{\pm} = \left\{ \boldsymbol{x} \in X : \boldsymbol{x} = \boldsymbol{s}_I(\boldsymbol{f}) \pm \sum_{k=1}^{n-N} \alpha_k(\boldsymbol{f}) \boldsymbol{v}_n^{(k)}(\boldsymbol{f}) \right\} \tag{3}$$

The surrogate model domain is then given as

$$X_S = \left\{ \begin{array}{c} \boldsymbol{x} = \boldsymbol{s}_I(\boldsymbol{f}) + \sum_{k=1}^{n-N} \lambda_k \alpha_k(\boldsymbol{f}) \boldsymbol{v}_n^{(k)}(\boldsymbol{f}) : \boldsymbol{f} \in F, \\ -1 \le \lambda_k \le 1, k = 1, \ldots, n-N \end{array} \right\} \tag{4}$$

The final (second-level) kriging surrogate is subsequently established within X_S with the training data set $\{\boldsymbol{x}_B^{(k)}, \boldsymbol{R}(\boldsymbol{x}_B^{(k)})\}_{k=1,\ldots,N_B}$.

It should be noted that the above definition of the model domain permits straightforward realization of uniform sampling within X_S. This is of fundamental importance for ensuring the best possible predictive power of the surrogate.

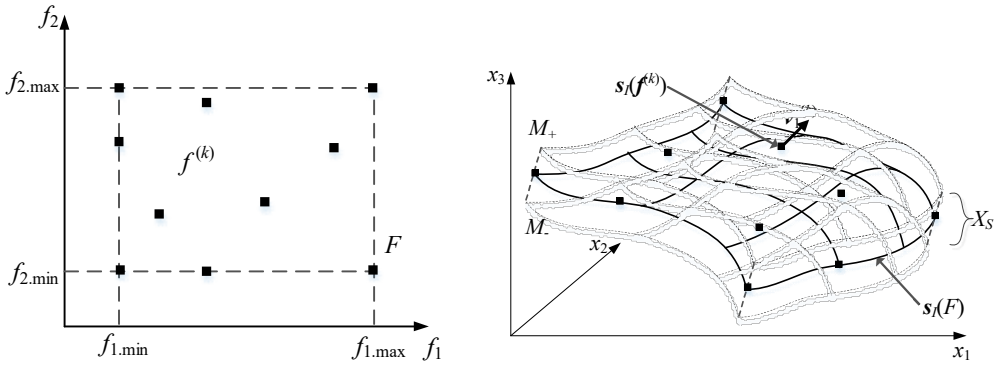

Fig. 1. Graphical illustration of the main components of the nested kriging modeling, here, explained for a two-dimensional objective space and three dimensional parameter space: (a) reference designs and objective space F; (b) the image $\boldsymbol{s}_I(F)$ of the first-level surrogate model and the normal vector $\boldsymbol{v}_1^{(k)}$ at $\boldsymbol{f}^{(k)}$; the manifolds M_- and M_+ as well as the surrogate model domain X_S defined as the orthogonal extension of $\boldsymbol{s}_I(F)$.

The exposition of the nested kriging modeling provided in this section is necessarily brief and only covers the aspects relevant to this work. More details can be found in Koziel and Pietrenko-Dabrowska, 2019.

2.4. Nested Kriging for Multi-Objective Design Framework

The major contributor to the computational cost of the surrogate-assisted framework of Section 2.1 is the acquisition of the training data for surrogate model construction (Koziel *et al.*, 2014a). It might be responsible for as much as 80 percent of the overall cost, which creates a room for improvements. In this work, we use the nested kriging approach outlined in Section 2.3 to implement a more efficient design space reduction (as compared to that of Section 2.2), but also to construct the surrogate model itself. The primary challenge of applying the nested kriging technique for MO is that the objective space constitutes merely a small part of an interval, e.g., a one-dimensional object (curve) in the case of $N_{obj} = 2$, or a fragment of a 2D surface in the case of $N_{obj} = 3$. This section explains how the technique can be adopted for our purposes while retaining its fundamental advantages mentioned in Section 2.3.

In the context of MO, the figures of interest f_k of the nested model are identical with the design objectives F_k of Section 2.1, and, consequently, $N = N_{obj}$. For "general" modeling, the reference designs were to be uniformly distributed within the interval-like objective space F. For the purpose of MO, they need to account for the Pareto front geometry (include the extreme designs $\boldsymbol{x}^{*(k)} = \text{argmin}\{\boldsymbol{x} : F_k(\boldsymbol{R}(\boldsymbol{x}))\}$ and additional designs if more detailed information is desired, e.g., the front curvature). Let us define $\boldsymbol{F}_k = [F_1(\boldsymbol{x}^{*(k)}) \ \ldots \ F_N(\boldsymbol{x}^{*(k)})]^T$, $k = 1, \ldots, N$. The generic way of obtaining the reference designs is to solve

$$\boldsymbol{x}^{\boldsymbol{w}} = \arg\min_{\boldsymbol{x}} F_1\left(\boldsymbol{R}(\boldsymbol{x})\right) \tag{5}$$

under the constraints

$$F_j(\boldsymbol{x}) \le \sum_{l=1}^{N} w_l F_j(\boldsymbol{x}^{*(l)}), \qquad j = 2,\ldots,N \tag{6}$$

where $\boldsymbol{w} = [w_1 \ \ldots \ w_N]^T$ is a vector of weights representing a convex combination, i.e.,

$$0 \le w_j \le 1 \quad \text{and} \quad \sum_{j=1}^{N} w_j = 1 \tag{7}$$

Note that the extreme Pareto-optimal designs $\boldsymbol{x}^{*(k)}$ correspond to the weighting vectors $\boldsymbol{w} = [0 \ \ldots \ 1 \ \ldots \ 0]^T$ with 1 on the kth position. Other arrangements would distribute the reference designs along the Pareto front; for example $\boldsymbol{w} = [1/N \ 1/N \ \ldots \ 1/N]^{\mathrm{T}}$ corresponds to the front center. Below, $\boldsymbol{F}(\boldsymbol{w})$ refers to the objective vector corresponding to the reference design $\boldsymbol{x}^{\boldsymbol{w}}$.

Let us now establish a mapping between the weighting vectors $\boldsymbol{w}$ (specifically, those satisfying (7)) and the part of the objective space corresponding to the Pareto front. First, for constructing the surrogate model and allocation of the training data, it is convenient to use an auxiliary transformation from a unit N–1 simplex S^{N-1} onto the space of the weights $\boldsymbol{w}$, defined as

$$h_0(\boldsymbol{z}) = \begin{bmatrix} 1 \\ 0 \\ \vdots \\ 0 \end{bmatrix} + \begin{bmatrix} -1 & -1 & \cdots & -1 \\ 1 & 0 & \cdots & 0 \\ 0 & 1 & \cdots & 0 \\ \vdots & \vdots & \ddots & \vdots \\ 0 & 0 & \cdots & 1 \end{bmatrix} \cdot \boldsymbol{z} \tag{8}$$

where

$$S^{N-1} = \left\{ \boldsymbol{z} = [z_1 \ldots z_{N-1}]^T : 0 \le z_k \le 1 \ \text{and} \ \sum_{k=1}^{N-1} z_k \le 1 \right\} \tag{9}$$

Figure 2 shows some illustrative examples of these concepts for the two- and three-objective cases. The thick dotted lines indicate the parts of the objective spaces where the

nested kriging model is to be established. A certain extension is necessary to accommodate the fact that only a rough approximation of the Pareto front geometry is given by the available reference designs, the number of which is very limited in practice. The extended region O (the actual domain of the first-level surrogate) is defined as the set of all points of the form

$$\boldsymbol{w} = h_0(\boldsymbol{z}) \cdot (1 + d) \quad \text{with} \quad \boldsymbol{z} \in S^{N-1} \quad \text{and} \quad -d_w \le d \le d_w \tag{10}$$

where d_w is the extension factor (here, we use $d_w = 0.05$).

The first-level surrogate for MO is established using the reference designs. It is a composition of two transformations: (i) the mapping from the Cartesian product of $S^{N-1} \times [-d_w, d_w]$ onto the objective space region O, and (ii) the "conventional" first-level model $\boldsymbol{s}_I$ of Section 2.3 from O into X. The former transformation is merely used for the sake of convenience: it is easier to implement uniform data sampling on $S^{N-1} \times [-d_w, d_w]$ rather than directly within O.

The second-level surrogate is subsequently set up in the domain constructed as in Section 2.3 but with $\boldsymbol{s}_I(O)$ being orthogonally extended instead of $\boldsymbol{s}_I(F)$. It should be emphasized that the Pareto front geometry is accurately identified through the variation of the nested modeling technique introduced in this section. The number of reference designs required for obtaining a reasonable Pareto front representation is up to three or four for $N_{obj} = 2$ (cf. Fig. 2(a)), and up to six or seven for $N_{obj} = 3$ (cf. Fig. 2(b)). Clearly, identification of the reference designs incurs certain computational expenses. However, the cost of finding additional reference designs (other than the extreme ones) is usually low because good initial points for finding $\boldsymbol{x}^w$ can be established as

$$\boldsymbol{x}^{\boldsymbol{w}(0)} = \sum_{l=1}^{N} w_l \boldsymbol{x}^{*(l)} \tag{11}$$

where $\boldsymbol{x}^{*(l)}$, $l = 1, \ldots, N$, are, as before, the extreme design corresponding to $\boldsymbol{w} = [0 \ldots 1 \ldots 0]^T$ with 1 on the lth position.

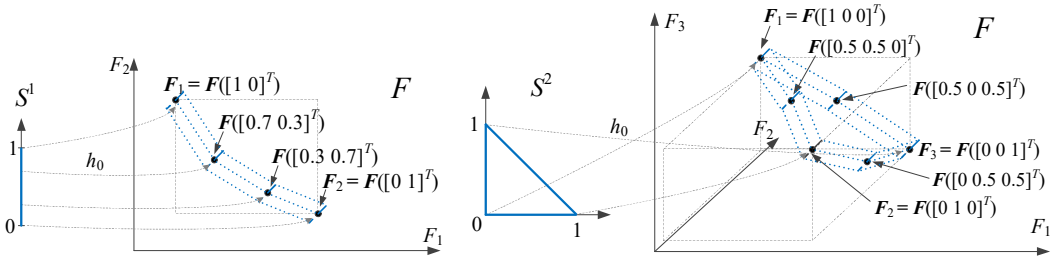

Fig. 2. Conceptual illustration of the objective space and the objective vectors corresponding to selected reference designs as well as the objective space regions (marked using dotted lines) where the nested kriging model is to be constructed. The mapping h_0 from the unity simplex onto the objective space region is also shown: (a) two-objective case, (b) three-objective case.

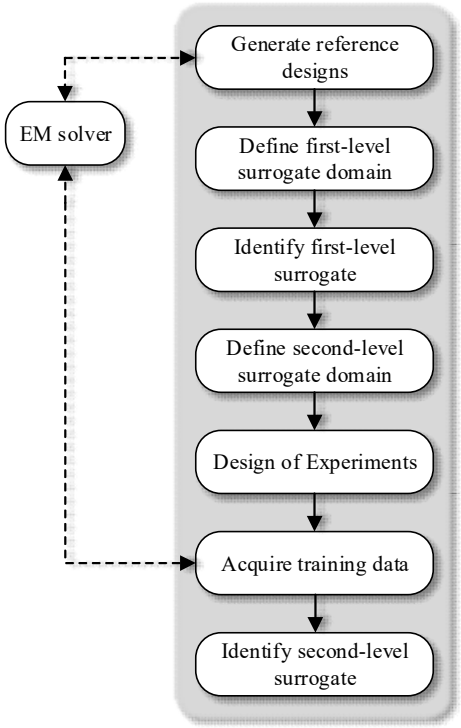

Fig. 3. Flow diagram of the nested surrogate modeling process for multi-objective optimization.

Figure 3 shows the flow diagram of the nested surrogate modeling process for MO. According to the surrogate-assisted procedure of Section 2.1, the second-level model is optimized using MOEA to yield the initial Pareto set, further refined using (1). Here, only high-fidelity EM simulations are used to proof the computational efficiency of the proposed methodology even without the usage of variable-fidelity simulations.

A few comments should be made about the surrogate model optimization. Formally, the surrogate is optimized in the original domain of the first-level surrogate, that is, $S^{N-1} \times [-d_w, d_w]$. For the sake of antenna evaluation, the designs $\boldsymbol{y} \in S^{N-1} \times [-d_w, d_w]$ are transformed into the weight vectors $\boldsymbol{w}$ using (10), and then into $\boldsymbol{x} \in X$ using the $\boldsymbol{s}_I$. This permits us to operate within a geometrically simple domain defined by the lower/upper bounds $0 \le y_k \le 1$, $k = 1, \ldots, N-1$, $-d_w \le y_N \le d_w$, and a linear constraint $\sum_{k=1,\ldots,N-1} y_k \le 1$, despite the actual shape of the Pareto front. The process of surrogate model evaluation has been shown in Fig. 4.

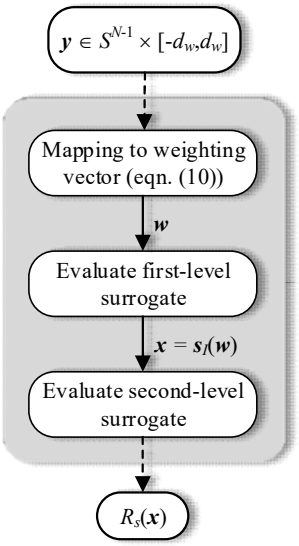

Fig. 4. Evaluation of the nested kriging surrogate for MO process. The model is operated from the domain $S^{N-1} \times [-d_w, d_w]$, and the argument $\boldsymbol{y}$ is first mapped into the space of the weighting vectors using (10), then into the surrogate model domain X_S (part of the antenna geometry parameter space), where the second-level surrogate is finally evaluated to yield the antenna responses.

3. Application Case Studies

The multi-objective optimization framework proposed in this paper is demonstrated here using two examples, a planar Yagi antenna and an ultra-wideband monopole antenna. For the first example, there are two objectives considered: improvement of the in-band matching and gain maximization. For the second example, we have three goals: improvement of the impedance matching, reduction of the in-band gain variability, and reduction of the antenna size. Our framework is compared to the benchmark surrogate-assisted MO algorithm of Section 2.1/2.2.

It should be noted that only high-fidelity EM simulations are utilized, therefore a direct comparison with variable-fidelity frameworks is not possible, although the proposed technique can be generalized to accommodate low- and high-fidelity EM simulations in a straightforward manner.

3.1. Case 1: Planar Yagi Antenna

The first demonstration example is a planar Yagi antenna shown in Fig. 5 (Kaneda *et al.*, 2002). The structure is implemented on RT6010 substrate (ε_r = 10.2, h = 0.635 mm) and comprises a driven element fed by a coplanar strip-line, director, and a microstrip balun. The antenna is fed with a 50 ohm microstrip. Design variables are $\boldsymbol{x} = [s_1\ s_2\ v_1\ v_2\ u_1\ u_2\ u_3\ u_4]^T$. Other parameters are fixed as follows: $w_1 = w_3 = w_4 = 0.6$, $w_2 = 1.2$, $u_5 = 1.5$, $s_3 = 3.0$ and $v_3 = 17.5$, all in mm. The computational model $\boldsymbol{R}$ is simulated in CST Microwave Studio (~600,000 mesh cells, simulation time 4 minutes) using its time domain solver.

The antenna is supposed to operate within the frequency range 10 GHz to 11 GHz. The figures of interest are minimization of in-band reflection (F_1) and maximization of the average end-fire gain (F_2), both within the operating bandwidth.

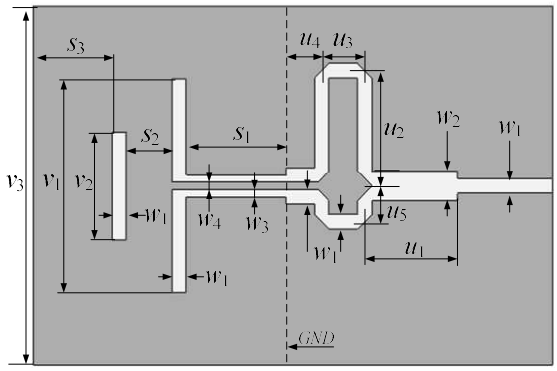

Fig. 5. Geometry of the planar Yagi antenna.

To set up the surrogate model we use four reference designs, corresponding to the two extreme designs $\boldsymbol{x}^{*(1)}$ = [4.43 3.85 8.77 4.28 4.09 4.76 2.08 1.63]^T, $\boldsymbol{x}^{*(2)}$ = [5.19 6.90 7.10 5.08 3.54 4.78 2.23 0.93]^T, and two more, corresponding to $\boldsymbol{z}$ = 0.33 and $\boldsymbol{z}$ = 0.66 (cf. (6)): $\boldsymbol{x}^{*(3)}$ = [4.56 4.38 8.56 4.50 3.89 4.93 2.01 1.57]^T, $\boldsymbol{x}^{*(4)}$ = [4.84 5.00 8.09 4.64 3.98 4.89 2.00 1.50]^T.

The thickness parameter was set to D = 0.05, which allows for achieving good predictive power of the surrogate while using a small number of training data points. The in-depth analysis of the dependence of the modeling error on the parameter D can be found in Koziel and Pietrenko-Dabrowska, 2019.

The nested kriging model was set up as outlined in Sections 2.3 and 2.4 using only 100 data samples. The relative RMS error of the surrogate (determined through cross validation) is 5% for the reflection response and 1% for the gain. The relative error is defined as $||\boldsymbol{R}(\boldsymbol{x}) - \boldsymbol{R}_s(\boldsymbol{x})||/||\boldsymbol{R}(\boldsymbol{x})||$, where $\boldsymbol{R}_s$ stands for the surrogate. The 10-fold cross-validation has been utilized (Queipo *et al.*, 2005)

In order to emphasize the benefits of the proposed approach, the surrogate was also constructed within the initially reduced space, i.e., the interval $\boldsymbol{l}^* = \min\{\boldsymbol{x}^{*(1)}, \boldsymbol{x}^{*(2)}\}$ and $\boldsymbol{u}^*$ =

max{$\boldsymbol{x}^{*(1)}$, $\boldsymbol{x}^{*(2)}$}. Despite of using 1600 training samples, the model error levels were much higher: 9% and 3% for reflection and gain characteristics, respectively.

The initial Pareto set found by optimizing the surrogate using MOEA is shown in Fig. 6 along with the selected designs evaluated through EM simulation, before and after the refinement process. The corresponding numerical data has been gathered in Table 1. Figure 7 shows the reflection and realized gain characteristics for the selected designs. Table 2 summarizes the optimization cost which includes finding the reference designs.

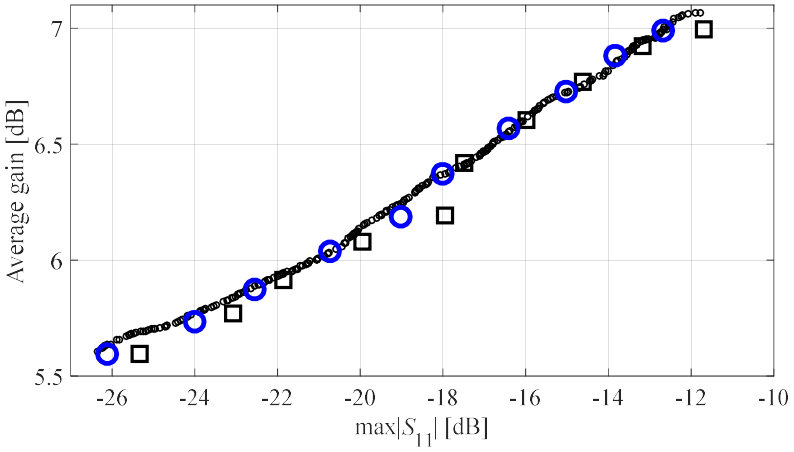

Fig. 6. Pareto-optimal solutions found for the Yagi antenna of Fig. 5 using the proposed methodology: (o) initial Pareto set identified using MOEA executed on the nested kriging surrogate, (□) EM-evaluated selected designs from the initial Pareto set, (O) EM-simulated refined Pareto designs.

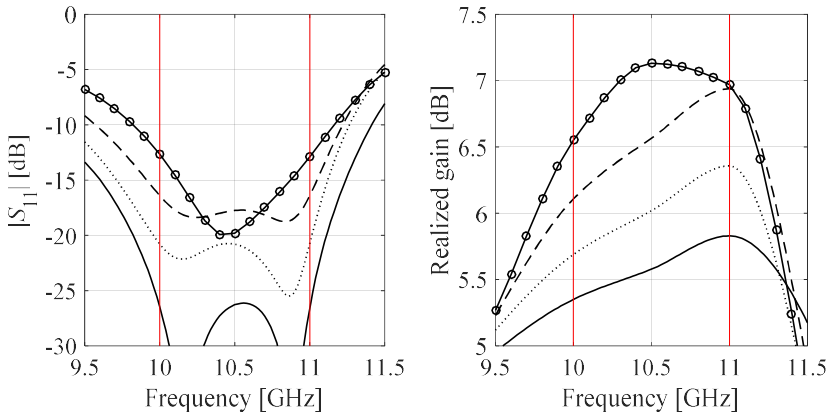

Fig. 7. Reflection (left) and realized gain (right) characteristics of the selected Pareto-optimal designs of Table 1: $\boldsymbol{x}^{(1)}$ (—), , $\boldsymbol{x}^{(4)}$ (····), $\boldsymbol{x}^{(7)}$ (- - -), and $\boldsymbol{x}^{(10)}$ (-o-).

Note that the major contributor is the training data acquisition for setting up the surrogate model which is dramatically reduced for the proposed framework (from 1600 to only 100 samples). This leads to lowering the total expenses by 80 percent. Also, the overall cost is just around 400 EM simulations despite the fact that single-fidelity models are utilized. Another advantage of our approach is a more precise identification of the initial Pareto set, which is due to a considerably smaller domain of the nested kriging model and better predictive power of the surrogate. This is illustrated in Fig. 8 that shows the initial Pareto set found using the surrogate established in the initially reduced design space. It can be observed that the span of the front obtained using the proposed methodology is considerably wider and of better quality (in terms of the objective function values) than the one yielded by the benchmark method. Even more importantly, significant discrepancies between the initial front, the EM-simulated objectives and the refined designs can be noticed, demonstrating the lack of surrogate model accuracy.

Table 1. Planar Yagi Antenna: Pareto-Optimal Designs

Design #	Design Variables [mm]								max $\|S_{11}\|$ [dB]	Gain* [dB]
	s_1	s_2	v_1	v_2	u_1	u_2	u_3	u_4		
1	4.41	3.88	8.78	4.25	4.05	4.78	2.07	1.60	–26.1	5.6
2	4.46	4.08	8.71	4.34	3.98	4.86	2.03	1.60	–24.0	5.7
3	4.52	4.25	8.64	4.44	3.91	4.90	2.03	1.58	–22.6	5.9
4	4.62	4.52	8.48	4.49	3.92	4.94	2.00	1.57	–20.7	6.0
5	4.76	4.74	8.26	4.56	4.00	4.91	2.00	1.56	–19.0	6.2
6	4.86	5.11	8.05	4.59	3.99	4.89	2.01	1.48	–18.0	6.4
7	4.93	5.50	7.86	4.66	3.92	4.88	2.05	1.38	–16.4	6.6
8	4.99	5.82	7.66	4.75	3.84	4.86	2.09	1.27	–15.0	6.7
9	5.08	6.30	7.41	4.86	3.72	4.83	2.16	1.13	–13.8	6.9
10	5.17	6.83	7.12	5.01	3.58	4.81	2.23	0.95	–12.7	7.0

* End-fire gain averaged over the 10-to-11 GHz bandwidth.

The selected designs have been fabricated and measured for additional verification. Figure 9 shows the photographs of the antenna prototypes, whereas Fig. 10 provides a comparison of the simulated and measured reflection and realized gain characteristics (these being design objectives considered in the optimization process). It can be observed that the agreement between the two sets of data is satisfactory.

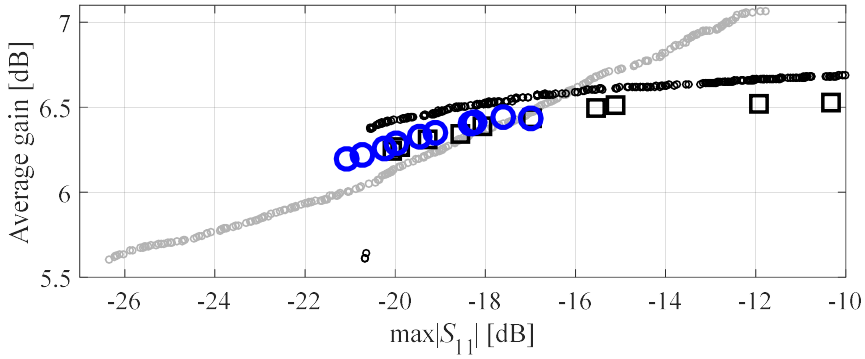

(a)

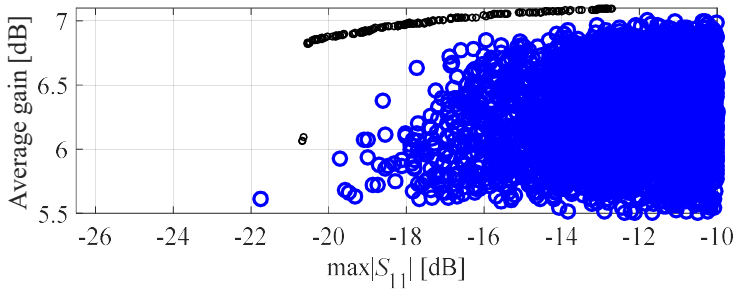

(b)

Fig. 8. (a) Pareto-optimal solutions found using the surrogate-assisted algorithm working with initial design space reduction (surrogate constructed within the interval [$\boldsymbol{l}^*$,$\boldsymbol{u}^*$]). (o) initial Pareto set identified using MOEA executed on the nested kriging surrogate, (□) EM-evaluated selected designs from the initial Pareto set, (O) EM-simulated refined Pareto designs. For comparison, the initial Pareto set found using the proposed methodology is shown using gray circles. Note considerably larger span of the Pareto set found using the nested kriging surrogate as well as better consistency between the initial and refined Pareto-optimal designs (cf. Fig. 6); (b) the approximate image of the initially reduced parameter space (large circles), i.e., the interval [$\boldsymbol{l}^*$ $\boldsymbol{u}^*$], obtained by randomly generating 10,000 points. It can be observed that the considered design objectives are indeed partially conflicting and the optimization process is required in order to identify the Pareto-optimal designs (small circles). Vast majority of the designs in the interval [$\boldsymbol{l}^*$ $\boldsymbol{u}^*$] are far from being optimal.

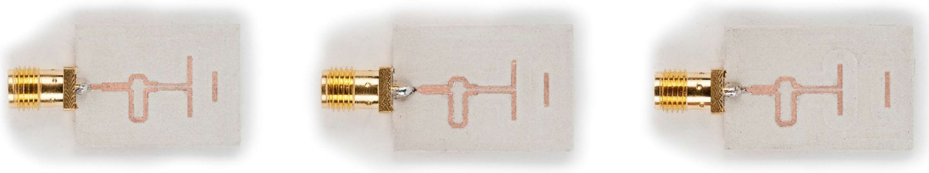

(a) (b) (c)

Fig. 9. Photographs of the fabricated prototypes of the Yagi antenna: (a) Design 1, (b) Design 5, (c) Design 10.

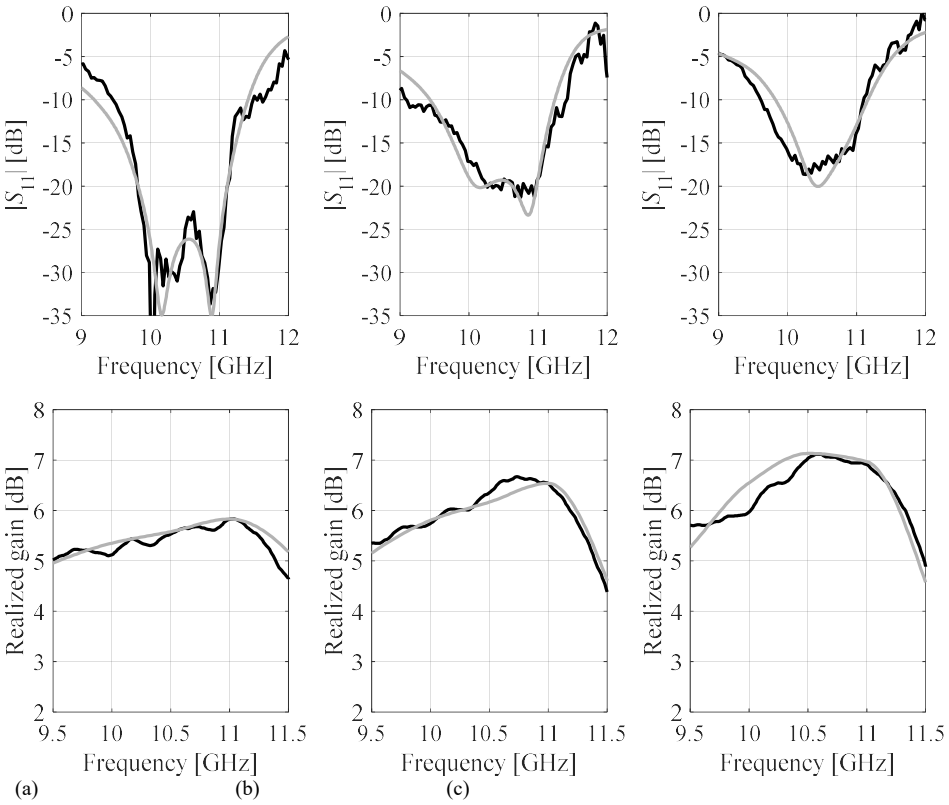

Fig. 10. Simulated (gray) and measured (black) reflection and realized gain characteristics of the fabricated Yagi antenna prototypes: (a) Design 1, (b) Design 5, (c) Design 10.

3.2. Case 2: Wideband Monopole Antenna

Our second example is the ultrawideband monopole antenna (Alsath and Kanagasabai, 2015) implemented on Taconic RF-35 substrate ($\varepsilon_r = 3.5$, $h = 0.762$ mm) and shown in Fig. 11. The independent geometry parameters for this structure are $\boldsymbol{x} = [L_0\ dR\ R\ r_{rel}\ dL\ dw\ L_g\ L_1\ R_1\ dr\ c_{rel}]^T$. The computational model is implemented in CST Microwave

Studio and evaluated using its transient solver (~840,000 mesh cells, simulation time 5 minutes). The EM model incorporates the SMA connector.

The antenna is to operate within the UWB band of 3.1 GHz to 10.6 GHz. Three figures of interest are considered: minimization of in-band reflection (F_1), reduction of the realized gain variability within the operating band (F_2), and reduction of the antenna size (F_3). As before, the thickness parameter was set to $D = 0.05$.

The surrogate model is set up using seven reference designs. These include three extreme designs (best matching, minimum gain variation, and minimum size): $\boldsymbol{x}^{*(1)}$ = [10.64 0.0 6.00 0.10 1.46 6.20 10.46 4.26 2.00 0.73 0.49]^T, $\boldsymbol{x}^{*(2)}$ = [8.74 1.55 5.81 0.51 0.016 5.65 8.95 5.47 2.60 0.99 0.84]^T, $\boldsymbol{x}^{*(3)}$ = [9.51 0.19 4.46 0.27 4.33 1.17 10.05 6.00 2.94 0.99 0.90]^T, and four more, corresponding to $\boldsymbol{z}$ = [0.0 0.5]^T, $\boldsymbol{z}$ = [0.5 0.0]^T, $\boldsymbol{z}$ = [0.5 0.5]^T, and $\boldsymbol{z}$ = [0.333 0.333]^T (cf. (6)): $\boldsymbol{x}^{*(4)}$ = [10.04 0.43 5.85 0.26 0.0 6.46 10.01 5.49 2.14 1.00 0.83]^T, $\boldsymbol{x}^{*(5)}$ = [9.58 0.0 5.05 0.28 3.37 4.14 9.68 5.26 2.37 0.85 0.89]^T, $\boldsymbol{x}^{*(6)}$ = [8.76 0.0 5.62 0.69 2.24 2.92 8.93 5.94 2.58 0.99 0.27]^T, $\boldsymbol{x}^{*(7)}$ = [9.52 0 .37 5.08 0.16 2.61 4.85 9.55 5.39 2.25 0.91 0.88]^T.

Table 2. Yagi Antenna: Optimization Cost Breakdown

Cost item	Surrogate model domain	
	X_S (this work)	Hypercube [$\boldsymbol{l}^*$,$\boldsymbol{u}^*$]
Extreme points	280 × $\boldsymbol{R}$	160 × $\boldsymbol{R}$
Data acquisition for kriging surrogate	100 × $\boldsymbol{R}$	1600 × $\boldsymbol{R}$
MOEA optimization*	N/A	N/A
Refinement	30 × $\boldsymbol{R}$	30 × $\boldsymbol{R}$
Total cost#	410 × $\boldsymbol{R}$ (27 h)	1790 × $\boldsymbol{R}$ (118 h)

* The cost of MOEA optimization is negligible compared to other stages of the process.
# The total cost is expressed in terms of the equivalent number of EM simulations.

The nested kriging model was set up using 200 data samples. The RMS error of the surrogate is 7.5% for the reflection response and 4% for the gain. For the sake of comparison, the surrogate was also constructed within the initially reduced space, i.e., the interval $\boldsymbol{l}^* = \min\{\boldsymbol{x}^{*(1)}, \boldsymbol{x}^{*(2)}\}$ and $\boldsymbol{u}^* = \max\{\boldsymbol{x}^{*(1)}, \boldsymbol{x}^{*(2)}\}$, using 1600 training samples. The obtained error values are much higher: 15% and 11% for reflection and gain characteristics, respectively. It should be noted that this case is considerably more difficult from the standpoint of surrogate model construction due to higher dimensionality of the parameter space (eleven variables vs. eight for the Yagi antenna) as well as wider parameter ranges.

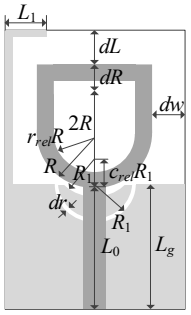

Fig. 11. Geometry of the ultrawideband monopole antenna (Alsath and Kanagasabai, 2015). The ground plane marked using the light gray shade.

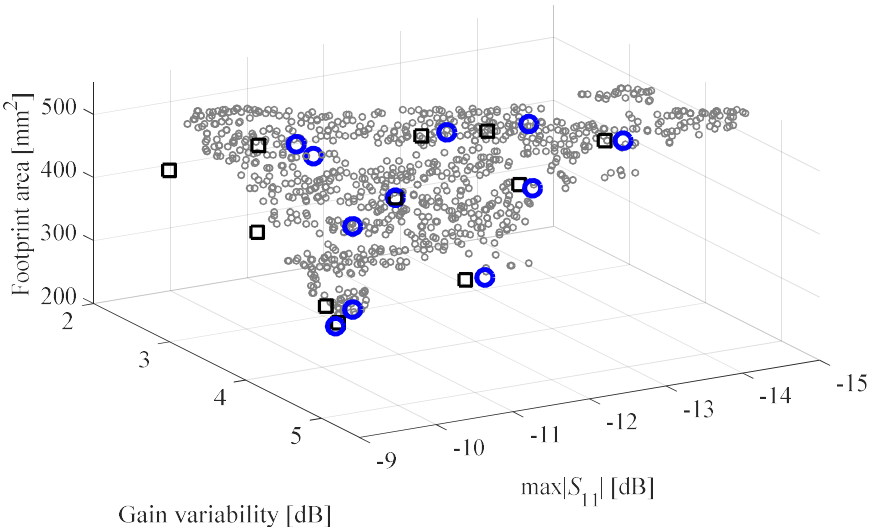

Fig. 12. Pareto-optimal solutions found for the UWB monopole antenna of Fig. 11 using the proposed methodology: (o) initial Pareto set identified using MOEA executed on the nested kriging surrogate, (□) EM-evaluated selected designs from the initial Pareto set, (O) EM-simulated refined Pareto designs.

Figure 12 shows the initial Pareto set found through MOEA-optimization of the nested kriging surrogate as well as the selected designs evaluated using EM simulation (before and after the refinement). Table 3 provides the numerical data, whereas Fig. 13 shows the reflection and realized gain characteristics for the selected designs. The optimization process cost breakdown has been given in Table 4. Similarly as for the first example, acquisition of the training data plays the major role and the proposed methodology allows us to reduce the overall expenses by over 50 percent. For this example, the nested kriging surrogate and the surrogate constructed in the initially reduced space lead to similar initial Pareto fronts as illustrated in Fig. 14 with the slightly wider span of the front for the latter model (this being a consequence of a larger model domain).

Table 3. UWB Antenna: Pareto-Optimal Designs

Design		1	2	3	4	5	6	7	8	9	10	11	12
max $\|S_{11}\|$ [dB]		–14.9	–10.5	–9.8	–12.2	–11.1	–12.9	–13.6	–12.5	–11.2	–11.3	–10.7	–10.1
Gain variability [dB]		4.8	3.1	4.4	3.5	2.8	3.7	4.3	4.3	4.9	3.6	3.7	4.3
Footprint area [mm^2]		564	487	292	497	441	508	508	453	373	418	387	308
Design variables	L_0	10.5	9.18	9.19	9.55	9.21	9.79	10.1	9.76	9.00	9.19	8.81	9.23
	dR	0.06	1.10	0.00	0.79	0.72	0.61	0.05	0.16	0.10	0.39	0.14	0.01
	R	5.88	5.52	4.91	5.52	5.26	5.51	5.61	5.29	5.19	5.20	5.51	4.95
	r_{rel}	0.16	0.33	0.43	0.38	0.31	0.21	0.27	0.32	0.51	0.30	0.69	0.38
	dL	1.49	0.55	3.88	0.37	1.44	0.41	1.66	2.63	3.30	2.48	2.35	4.04
	Dw	6.12	5.78	1.55	6.06	4.95	6.29	5.56	4.69	3.09	4.24	3.30	1.79
	L_g	10.3	9.18	9.77	9.58	9.33	9.75	10.0	9.78	9.35	9.31	9.08	9.74
	L_1	4.57	5.53	6.00	5.46	5.51	5.53	5.02	5.19	5.86	5.51	5.95	6.00
	R_1	2.05	2.42	2.81	2.30	2.32	2.24	2.12	2.27	2.59	2.34	2.59	2.78
	dr	0.81	1.00	1.00	1.00	0.97	0.99	0.91	0.85	0.96	0.98	1.00	0.99
	c_{rel}	0.58	0.90	0.67	0.85	0.74	0.78	0.69	0.84	0.55	0.70	0.29	0.71

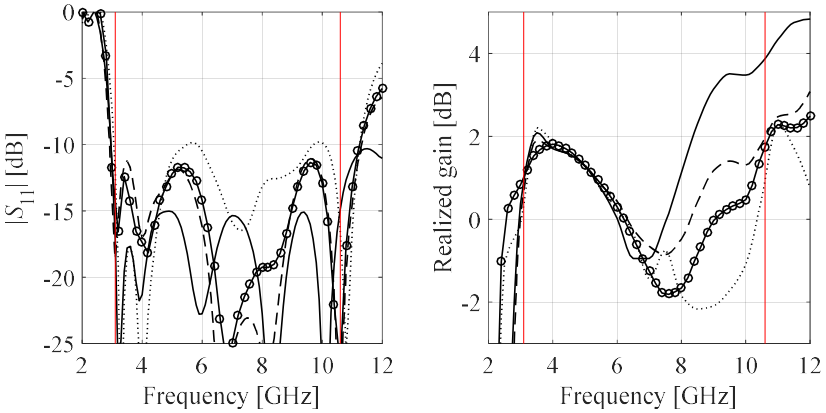

Fig. 13. Reflection (left) and realized gain (right) characteristics of the selected Pareto-optimal designs of Table 3: $\boldsymbol{x}^{(1)}$ (—), , $\boldsymbol{x}^{(3)}$ (····), $\boldsymbol{x}^{(5)}$ (- - -), and $\boldsymbol{x}^{(10)}$ (-o-).

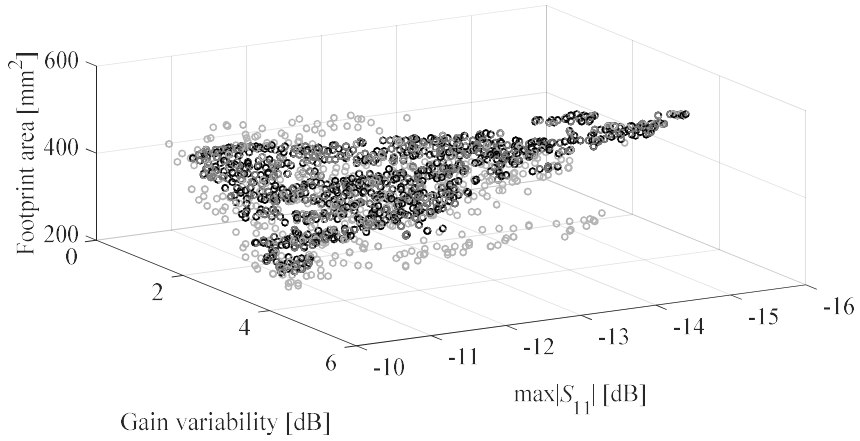

(a)

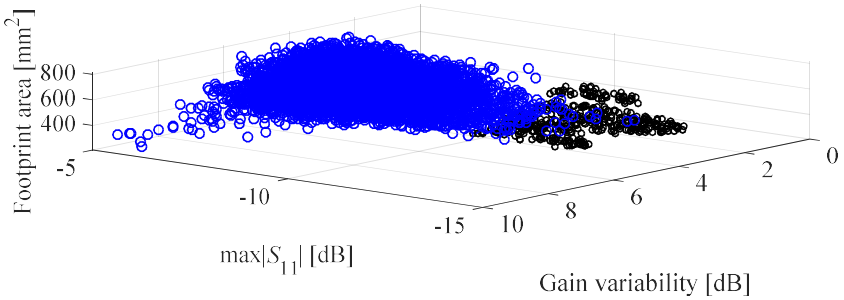

(b)

Fig. 14. (a) Initial Pareto sets obtained using the proposed methodology (black) and the surrogate model established in the initially reduced design space (the interval $[\boldsymbol{l}^*,\boldsymbol{u}^*]$) (gray). It can be observed that the Pareto front span is similar in both cases (slightly larger for the initially reduced space due to its considerably larger volume);); (b) the approximate image of the initially reduced parameter space (large circles), i.e., the interval $[\boldsymbol{l}^*\ \boldsymbol{u}^*]$, obtained by randomly generating 10,000 points. Similarly as for the previous example, it can be observed that the considered design objectives are indeed partially conflicting and the optimization process is required in order to identify the Pareto-optimal designs (small circles). Vast majority of the designs in the interval $[\boldsymbol{l}^*\ \boldsymbol{u}^*]$ are far from being optimal.

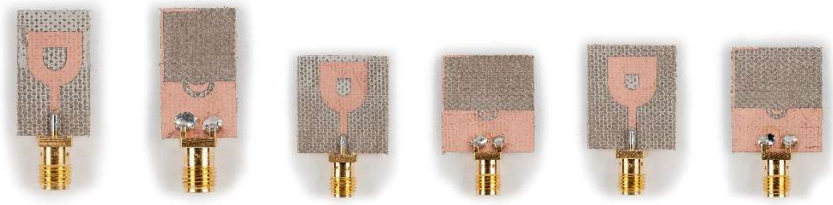

(a) (b) (c)

Fig. 15. Photographs of the fabricated prototypes of the UWB monopole: (a) Design 3, (b) Design 5, (c) Design 10.

Table 4. UWB Antenna: Optimization Cost Breakdown

Cost item	Surrogate model domain	
	X_S (this work)	Hypercube $[\boldsymbol{l}^*,\boldsymbol{u}^*]$
Extreme points	750 × ***R***	440 × ***R***
Data acquisition for kriging surrogate	200 × ***R***	1600 × ***R***
MOEA optimization*	N/A	N/A
Refinement	36 × ***R***	36 × ***R***
Total cost#	986 × ***R*** (82 h)	2076 × ***R*** (173 h)

* The cost of MOEA optimization is negligible compared to other stages of the process.
# The total cost is expressed in terms of the equivalent number of EM simulations.

Selected Pareto-optimal designs of the antenna of Fig. 11 have been fabricated and measured. Figure 15 shows the photographs of the antenna prototypes. The relevant antenna characteristics, i.e., reflection and realized gain, are shown in Fig. 16. The agreement between simulations and measurements is satisfactory.

4. Conclusion

In the paper, a technique for computationally efficient multi-objective design optimization of antenna structures has been proposed. Our methodology adopts a nested kriging modeling approach to identify a region of the design space that contains the best trade-off designs, and to set up—within that region—a fast surrogate model utilized to yield an initial approximation of the Pareto set. A rigorous formalism has been introduced

to generalize the nested kriging framework and apply it over an arbitrary subset of the objective space instead of the interval (as in the original formulation of the method).

The resulting framework has been comprehensively validated using two antenna examples, a planar Yagi and a UWB monopole, optimized for two and three objectives, respectively. It has been demonstrated that the proposed framework offers significant reduction of the computational cost of up to 80 percent as compared to the state-of-the-art surrogate-assisted approach while retaining or even improving the quality of Pareto front representation.

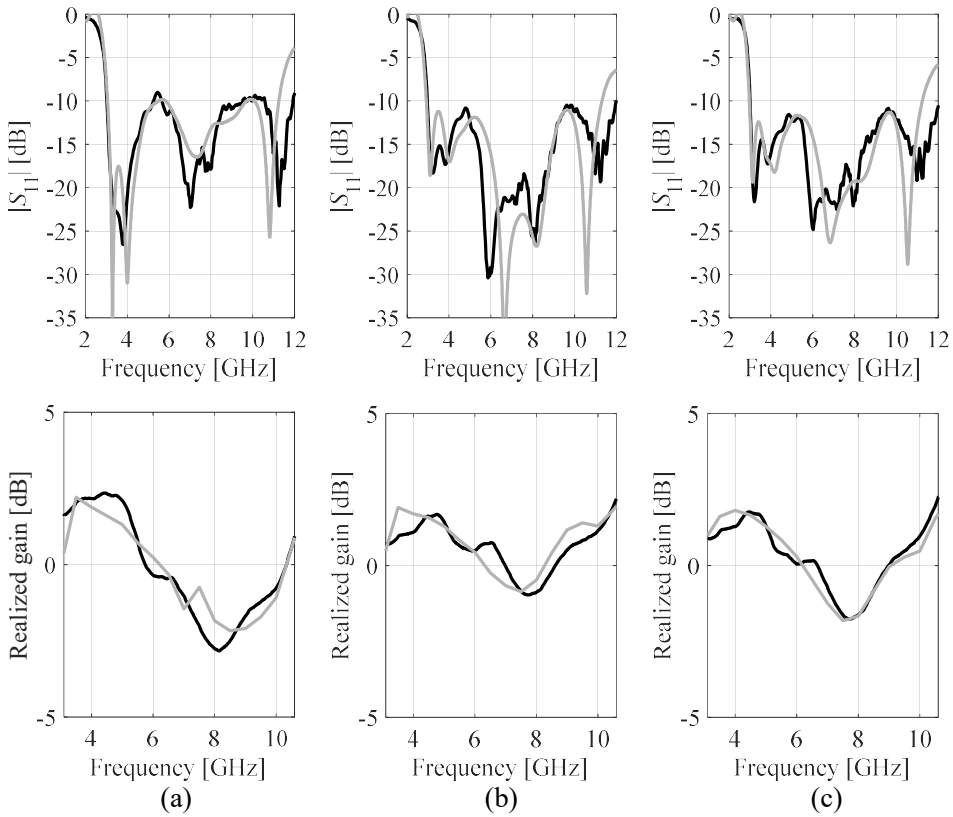

Fig. 16. Simulated (gray) and measured (black) reflection and realized gain characteristics of the fabricated UWB monopole prototypes: (a) Design 3, (b) Design 5, (c) Design 10.

In this work, the entire optimization process was intentionally carried out using exclusively high-fidelity EM simulation models. This was to demonstrate that even within this setup, the computational overhead of the multi-objective optimization process can be manageable. The future work will include generalizations of the proposed methodology incorporating variable-fidelity simulations.

Acknowledgement

The authors would like to thank Dassault Systemes, France, for making CST Microwave Studio available.

References

Akinsolu, M.O., Liu, B., Grout, V., Lazaridis, P.I., Mognaschi, M.E. and Di Barba, P. (2019). "A parallel surrogate model assisted evolutionary algorithm for electromagnetic design optimization," *IEEE Trans. Emerging Topics Comput. Intell.*, Vol. 3, No. 2, pp. 93-105.

Alsath, M.G.N. and Kanagasabai, M. (2015). "Compact UWB monopole antenna for automotive communications," *IEEE Trans. Ant. Prop.*, Vol. 63, No. 9, pp. 4204-4208.

An, S., Yang, S. and Mohammed, O.A. (2018). "A Kriging-assisted light beam search method for multi-objective electromagnetic inverse problems," *IEEE Trans. Magn.*, Vol. 54, No. 3, pp. 1-4.

Aravanis, A.I., Bhavani Shankar, M.R., Arapoglou, P., Danoy, G., Cottis, P.G. and Ottersten, B. (2015). "Power allocation in multibeam satellite systems: a two-stage multi-objective optimization," *IEEE Trans. Wireless Comm.*, Vol. 14, No. 6, pp. 3171-3182.

Bauernfeind, T., Baumgartner, P., Biro, O., Magele, C.A., Preis, K. and Torchio, R. (2017). "PEEC-based multi-objective synthesis of non-uniformly spaced linear antenna arrays," *IEEE Trans. Magn.*, Vol. 53, No. 6.

Bhattacharya, R., Garg, R. and Bhattacharyya, T.K. (2016). "Design of a PIFA-driven compact Yagi-type pattern diversity antenna for handheld devices," *IEEE Ant. Wireless Propag. Lett.*, Vol. 15, pp. 255-258, 2016.

Borhani, M., Rezaei, P. and Valizade, A. (2016). “Design of a reconfigurable miniaturized microstrip antenna for switchable multiband systems,” *IEEE Ant. Wireless Propag. Lett.*, Vol. 15, pp. 822-825.

Buckley, J.L., McCarthy, K.G., Loizou, L., O'Flynn, B. and O'Mathuna, C. (2016). “A dual-ISM-band antenna of small size using a spiral structure with parasitic element,” *IEEE Ant. Wireless Propag. Lett.*, Vol. 15, pp. 630-633.

Chauhan, N.C., Kartikeyan, M.V. and Mittal, A. (2012). *Soft computing methods for microwave and millimeter-wave design problems*. Studies in Computational Intelligence, Vol. 392, Springer, Berlin, Heidelberg.

Chen, Y.S. (2015). “Application of multi-objective fractional factorial design for ultra-wideband antennas with uniform gain and high-fidelity,” *IET Microwaves, Ant. Prop.*, Vol. 9, No. 15, pp. 1667-1672.

Darvish, A. and Ebrahimzadeh, A. (2018). “Improved fruit-fly optimization algorithm and its applications in antenna array synthesis,” *IEEE Trans. Ant. Prop.*, Vol. 66, No. 4, pp. 1756-1766.

Deb, K. (2001). *Multi-Objective Optimization Using Evolutionary Algorithms.* Wiley, New York.

Deb, K. and Gupta, H. (2006). “Introducing robustness in multi-objective optimization,” *EVol. Comput*., Vol. 14, No. 4, pp. 463-494.

Easum, J.A., Nagar, J. and Werner, D.H. (2017). “Multi-objective surrogate-assisted optimization applied to patch antenna design,” *Int. Symp. Ant. Prop.*, pp. 339-340, San Diego, USA.

Easum, J.A., Nagar, J., Werner, P.L. and Werner, D.H. (2018). “Efficient multi-objective antenna optimization with tolerance analysis through the use of surrogate models,” *IEEE Trans. Ant. Propag.*, Vol. 66, No. 12, pp. 6706-6715.

Fonseca, C.M. (1995). “Multiobjective genetic algorithms with application to control engineering problems,” PhD thesis, Department of Automatic Control and Systems Engineering, University of Sheffield, Sheffield, UK.

Goudos, S.K., Siakavara, K., Samaras, T., Vafiadis, E.E. and Sahalos, J.N. (2011) “Self-adaptive differential evolution applied to real-valued antenna and microwave design problems,” *IEEE Trans. Antennas Propag.*, Vol. 59, No. 4, pp. 1286–1298.

Jacobs, J.P. (2012). “Bayesian support vector regression with automatic relevance determina-tion kernel for modeling of antenna input characteristics,” *IEEE Trans. Antennas. Prop.*, Vol. 60, No. 4, pp. 2114-2118.

Jayaprakasam, S., Abdul Rahim, S.K., Leow, C.Y. and Mohd Yusof, M.F. (2014). "Beampatten optimization in distributed beamforming using multiobjective and metaheuristic method," *IEEE Symp. Wireless Techn. App. (ISWTA)*, Kota Kinabalu, Malaysia, pp. 86-91.

Kaneda, N., Deal, W.R., Qian, Y., Waterhouse, R. and Itoh, T. (2002). "A broad-band planar quasi Yagi antenna," *IEEE Trans. Antennas Propag.*, Vol. 50, pp. 1158-1160.

Koziel, S. and Bekasiewicz, A. (2015). „Rotational design space reduction for cost-efficient multi-objective antenna optimization," *Europ. Conf. Ant. Prop.*, Lisbon, Portugal, pp. 1-4.

Koziel, S. and Bekasiewicz, A. (2016). *Multi-Objective Design of Antennas Using Surrogate Models*, World Scientific, Singapore.

Koziel, S. and Ogurtsov, S. (2013). "Multi-objective design of antennas using variable-fidelity simulations and surrogate models," *IEEE Trans. Antennas Prop.*, Vol. 61, No. 12, pp. 5931-5939.

Koziel, S. and Ogurtsov, S. (2014). "Design optimization of antennas using electromagnetic simulations and adaptive response correction technique," *IET Microwaves, Antennas Prop.*, Vol. 8, No. 3, pp. 180-185.

Koziel, S. and Pietrenko-Dabrowska, A. (2019). "Performance-based nested surrogate modeling of antenna input characteristics," *IEEE Trans. Ant. Prop.*, Vol. 67.

Koziel, S. and Sigurdsson, A.T. (2017) "Triangulation-based constrained surrogate modeling of antennas," *IEEE Trans. Ant. Prop.*, Vol. 66, No. 8, pp. 4170-4179.

Koziel, S., Bekasiewicz, A. and Zieniutycz, W. (2014a). "Expedited EM-driven multi-objective antenna design in highly-dimensional parameter spaces," *IEEE Antennas and Wireless Prop. Lett.*, Vol. 13, pp. 631-634.

Koziel, S., Cheng, Q.S. and Bandler, J.W. (2008). "Space mapping," *IEEE Microwave Magazine*, Vol. 9, No. 6, pp. 105-122.

Koziel, S., Cheng, Q.S. and Li, S. (2018). "Optimization-driven antenna design framework with multiple performance constraints," *Int. J. RF Microwave CAE*, Vol. 28, No. 4.

Koziel, S., Bekasiewicz, A., Couckuyt, I. and Dhaene, T. (2014b). "Efficient multi-objective simulation-driven antenna design using co-kriging," *IEEE Trans. Antennas Prop.*, Vol. 62, No. 11, pp. 5900-5905.

Liu, B., Akinsolu, M.O., Ali, N. and Abd-Alhameed, R. (2018). "Efficient global optimisation of microwave antennas based on a parallel surrogate model-assisted

evolutionary algorithm," *IET Microwaves, Antennas & Propagation*, Vol. 13, No. 2, pp. 149-155.

Liu, J., Esselle, K.P., Hay, S.G. and Zhong, S. (2014). "Effects of printed UWB antenna miniaturization on pulse fidelity and pattern stability," *IEEE Trans. Ant. Prop.*, Vol. 62, No. 8, pp. 3903-3910.

Lyu, W., Yang, F., Yan, C., Zhou, D. and Zeng, X. (2018). "Multi-objective Bayesian optimization for analog/RF circuit synthesi," *ACM/ESDA/IEEE Design Autom. Conf.*, San Francisco, USA.

Matekovits, L., Laza, V.A. and Vecchi, G. (2007). "Analysis of large complex structures with the synthetic-functions approach," *IEEE Trans. Ant. Propag.*, Vol. 55, No. 9, pp. 2509-2521, 2007.

Mishra, S., Yadav, R.N., and Singh, R.P. (2015). "Directivity estimations for short dipole anten-na arrays using radial basis function neural networks," *IEEE Ant. Wireless Propag. Lett.*, Vol. 14, pp. 1219-1222.

Nagar, J. and Werner, D.H. (2018). "Multi-objective optimization for electromagnetics and optics: an introduction and tutorial," *IEEE Ant. Propag. Mag.*, Vol. 60, No. 6, pp. 58-71.

Na, W., Feng, F., Zhang., C., and Zhang., Q.J. (2017). "A unified automated parametric modeling algorithm using knowledge-based neural network and l_1 optimization," *IEEE Trans. Microwave Theory Techn.*, Vol. 65, no. 3, pp. 726-745.

Queipo, N.V., Haftka, R.T., Shyy, W., Goel, T., Vaidynathan, R., Tucker, P.K. (2005). "Surrogate based analysis and optimization", *Prog. Aerospace Sci.*, Vol. 41, pp. 1-28.

Rasmussen, C.E., and Williams, C.K.I. (2006). *Gaussian processes for machine learning*. MIT Press, Cambridge, MA, USA.

Rinaldo, R., Maufroid, X. and Garcia, R.C. (2005). "Non-uniform bandwidth and power allocation in multi-beam broadband satellite systems", *Proc. 23rd AIAA ICSSC*, Rome, Italy.

Simpson, T.W., Pelplinski, J.D., Koch, P.N. and Allen, J.K. (2001). "Metamodels for computer-based engineering design: survey and recommendations", *Engineering with Computers*, Vol. 17, pp. 129-150.

Soltani, S., Lotfi, P. and Murch, R.D. (2017). "A dual-band multiport MIMO slot antenna for WLAN applications," *IEEE Ant. Wireless Propag. Lett.*, Vol. 16, pp. 529-532.

Stutzman, W.L. and Thiele, G.A. (2012). *Antenna Theory and Design*, 3rd ed., Wiley, New York.

Szini, I., Tatomirescu, A. and Pedersen, G.F. (2015). “On small terminal MIMO antennas, harmonizing characteristic modes with ground plane geometry,” *IEEE Trans. Ant. Propag.*, Vol. 63, No. 4, pp. 1487-1497.

Tian, B., Li, Z. and Wang, C. (2010). “Boresight gain optimization of an UWB monopole antenna using FDTD and genetic algorithm,” *IEEE Int. Conf. Ultra-Wideband*, Nanjing, China, pp. 1-4.

de Villiers, D.I.L., Couckuyt, I. and Dhaene, T. (2017). “Multi-objective optimization of reflector antennas using kriging and probability of improvement”, *Int. Symp. Ant. Prop.*, San Diego, USA, pp. 985-986.